Development of a grinding model based on flotation performance

Mathe Enoque, Cruz Constanza, Lucay Freddy A., Gálvez Edelmira D., Cisternas Luis A.

DOI: 10.1016/j.mineng.2021.106890

Development of a grinding model based on flotation performance

Enoque Mathe[1], Constanza Cruz[1,2], Freddy A. Lucay[3], Edelmira D. Gálvez[4], Luis A. Cisternas[1,*]

[1]Departamento de Ingeniería Química y Procesos de Minerales, Universidad de Antofagasta, Antofagasta, Chile
[2]School of Engineering Science, Lappeenranta-Lahti University of Technology (LUT University), Lappeenranta, Finland
[3]Escuela de Ingeniería Química, Pontificia Universidad Católica de Valparaíso, Chile
[4]Departamento de Ingeniería Metalúrgica y Minas, Universidad Católica del Norte, Antofagasta, Chile
[*] Corresponding author: luis.cisternas@uantof.cl; Tel.: +56-991384556

Abstract

Usually, the concentration of minerals is carried out with a set of flotation and grinding units. Most of the modeling strategies for the flotation and grinding stages have followed separate developmental paths. This paper presents a strategy based on using flotation studies to model flotation and grinding via an integrated approach. The methodology, which is an approximate method that allows one to study of the effects of grinding on flotation circuits, is applied to a copper sulfide mineral with appropriate results. Given its nature, the application of this method will help preliminary studies on the design, improvement, and simulation of flotation circuits. The major advantages of this method are its simplicity and low cost. Thus, the main contribution of this work is a new strategy to model grinding for integration into the modeling of flotation circuits. This new strategy can be extended to other concentration technologies that include grinding.

Keywords: modeling, flotation circuit, grinding circuit, process design

1. Introduction

Flotation is the most widely used technology in mineral processing, and thousands of tons of ore are produced worldwide every day. This technology's application affects several minerals, including sulfide minerals of lead, zinc, molybdenum, and copper, which are either polymetallic or not (Agheli et al., 2018; Prakash et al., 2018; Shean and Cilliers, 2011). Given the large-scale production of ore concentrates, a small improvement in recovery or product quality can produce a large increase in revenue. Therefore, permanent improvements are sought to increase recovery and reduce gangue in concentrates (Asghari et al., 2019; Kupka and Rudolph, 2018). Flotation processes include several flotation stages, with a specific configuration called a flotation circuit. The flotation circuit plays an important role in the observed recovery of valuable species and in the grade of concentrates. It has been shown that certain flotation circuits may be superior to others in terms of their economic gains, despite large variations in the recovery at each flotation stage (Cisternas et al., 2015). In other words, efforts to achieve better operating conditions—for example, with better collectors or foam handling—are marginal compared to the selection importance of the circuit structure. Whereas each flotation stage can include several flotation cells, the set of circuit

alternatives for a given problem can total thousands, millions, or even billions of possibilities (Hu et al., 2013; Sepúlveda et al., 2017). For this reason, it is not possible to examine all possibilities through experimentation. The simulation of flotation circuits could be a good alternative, as demonstrated in several studies (Montenegro et al., 2013; Yianatos et al., 2012). Flotation circuits usually consider regrinding stages to liberate valuable species from the gangue. However, most flotation circuit simulation strategies cannot be applied to grinding operations, thus limiting their application.

The modeling of flotation stages and grinding stages has followed different directions, which makes the simulation and design of flotation circuits difficult. There are several models for flotation kinetics, and several reviews have analyzed these models (Gharai and Venugopal, 2015; Jovanović et al., 2015; Jovanović and Miljanović, 2015; Mendez et al., 2009; Polat and Chander, 2000; Yianatos and Henríquez, 2006). First-order kinetic models are the most commonly used model, both in the literature and in practice. In these models, the flotation system is represented by species, where a species refers to a group of particles that have the same floatability or can be represented by the same kinetics. Mostly, these species are minerals classified as slow or fast (D. Kelsall, 1961; Sutherland, 1989, 1977). In the fast fraction, the particles are of medium size, whereas in the slow fraction, the particles are fine and coarse (Bu et al., 2017). Notably, the first-order kinetic model has been extended to consider multiple components, namely, multiple fractions, with each one having its own kinetics (Nguyen, 2003). This type of model has the advantage of better adjusting to flotation kinetics that integrate with a distribution of flotation constants (Polat and Chander, 2000). The central purpose of grinding models is to obtain mathematical relationships between the size of the feed and the size of the product (Monov et al., 2012). Size reduction is a result of three fragmentation mechanisms: abrasion, cleavage, and fracturing (Hennart et al., 2009). Different size classes are used because the grinding system includes particles that differ significantly in size. In the theory of the breakage of solids, the fragmentation process is decomposed into the selection of a fraction of the material to be broken and the breakage of the selected material, producing a given distribution of fragment sizes (Varinot et al., 1997). These two operations are characterized by selection and breakage functions. Three types of models are commonly accepted in the literature: matrix, kinetic, and energy models (Toneva and Peukert, 2007). A general principle in the development of each model is to establish mass balance or energy balance equations relating to the mass components or the energy involved in the process. Since the main objective of the grinding process is to obtain a desired particle size distribution in the final product, most models focus on particle size, an important variable for flotation, but it is insufficient in terms of relating grinding to flotation. Other models have been developed to include mineral liberation. However, in these models, the classes are defined based on particle size and liberation (Pérez-García et al., 2018), which can yield a large number of classes. Furthermore, the identification of the liberation can require expensive characterization analysis, e.g., QEMSCAN. Sosa-Blanco et al. (Sosa-Blanco et al., 1999) presented a procedure to simulate a grinding–flotation system. They applied a population balance model to describe the grinding, classification, and flotation processes. In the grinding model, particles were characterized by their size, while in the flotation models, particles were

characterized by their size and mineral composition. The link between grinding and flotation circuits was made using an empirical model that generates the mineral size particle population from the size distribution of the grinding circuit product. Once again, a large amount of experimentation is needed because of the representation by particle size and mineral composition.

Thus, because most flotation circuit simulation strategies cannot be applied to grinding operations, and vice versa, most studies on flotation circuits do not include grinding operations (Cisternas et al., 2018). For example, Méndez et al. (Mendez et al., 2015) modeled the flotation kinetics of an ore using a three-component kinetic model, redesigning a zinc flotation circuit using mathematical modeling techniques. Similarly, Calisaya et al. (Calisaya et al., 2016) applied the slow/fast model to design flotation circuits. However, both works did not consider grinding. Another method, linear circuit analysis (Meloy, 1983, 1983; Noble et al., 2019; Williams et al., 1986), also does not consider grinding. Unfortunately, predictive models are not available; therefore, the models used in practice are empirical and depend on the designed circuit. This is like the paradox of the chicken or the egg, where the circuit structure is required to determine the conditions to develop the flotation and grinding models, but the circuit structure cannot be developed without the flotation and grinding models. Because this is an iterative process, models that include particle size and liberation are too expensive. Significantly, it was demonstrated that accurate flotation and grinding models are not needed to identify the most optimal structures (Acosta-Flores et al., 2020, 2018; Calisaya et al., 2016; Cisternas et al., 2015). Therefore, only approximate values for recovery in each flotation stage and particle size conversion in grinding are required to obtain a set of optimal solutions. Consequently, approximate and straightforward models can be useful for circuit structure identification and preliminary evaluation when processing a new ore or an ore with new mineralogy.

This work aims to develop a procedure for the modeling of grinding units based on a representation of the system by species with low and fast flotation kinetics. The procedure is intended for approximate simulation and could be applied to preliminary simulation, operation, and design problems for grinding units that operate together with flotation units.

2. Methodology

The proposed methodology is based on the use of a flotation kinetics modeling strategy to represent ore grinding indirectly (see Figure 1). The idea is to consider the change in flotation kinetics that occurs between different species of particles before and after grinding. The species are represented by fine–slow, medium–fast, and coarse–slow particles. The change in the faction of fine–slow, medium–fast, and coarse–slow particles in flotation kinetics is considered to be a direct effect of the grinding stage. Then, based on this information, the grinding unit is modeled. The present methodology considers three steps: 1) Modeling the effect of time or energy on the particle size distribution in grinding based on grinding tests; 2) observing the impact of grinding on the flotation kinetics by using experimental tests at different times or energies used for grinding; and 3) modeling the fine–slow, medium–fast, coarse–slow grinding fractions based on flotation kinetics. Note that the grinding species fractions are indirectly determined based on the flotation results. These steps are described in the following subsections.

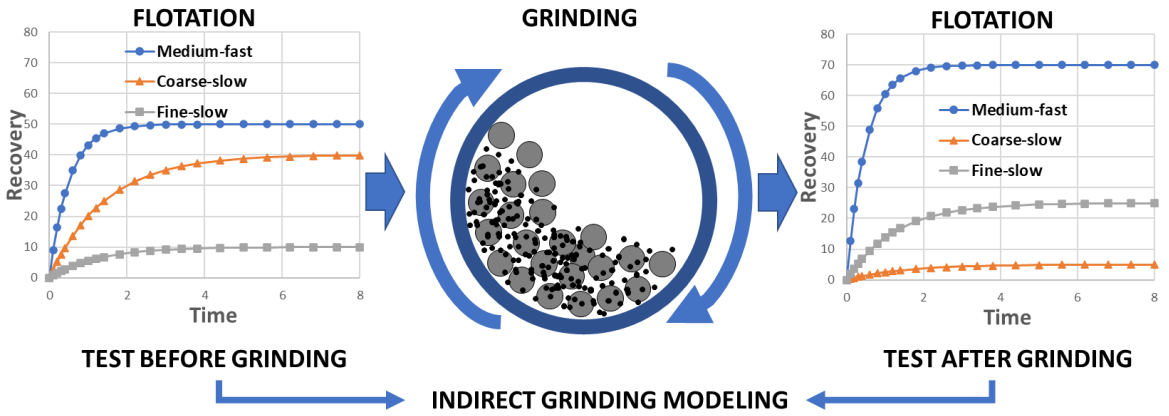

Figure 1. Representation of the modeling strategy.

2.1 Modeling particle size distribution

In mineral processing, the best known and most widely used distribution function is the particle distribution function $P(\Phi)$, where Φ is the particle size (King, 2003). $P(\Phi)$ is defined by the mass fraction of the portion of the population that consists of particles with a size less than or equal to Φ. There are several particle distribution functions, several of which can be used. Here, we propose to use the Rosin–Rammler–Bennett (RRB) distribution function, which is one of the most commonly used in practice and is suitable for small particle sizes (Alderliesten, 2013; Delagrammatikas and Tsimas, 2004). The RRB distribution is defined by the following equation:

$$P(\Phi) = 1 - \exp\left(-\left(\frac{\Phi}{K}\right)^{n}\right). \quad (1)$$

We consider that n, the spread parameter ($n > 0$), is a constant that depends on the ore analyzed, and K, the location parameter, is a parameter that is a function of the time (t_G) or energy in the grinding process. This is represented by the following equation:

$$K = \alpha\, t_G^{\beta} \quad (2)$$

where α and β are adjustable parameters. The values of $P(\Phi)$ are measured experimentally at a number of fixed sizes that correspond to the mesh sizes of the set of sieves available in the laboratory. The sizes of the mesh are determined based on the typical particle values in the flotation of a specific mineral. The experiments are run several times (or with varying energy) to model $K = f(t_G)$ or $K = f(E_G)$, where t_G and E_G are the time and energy needed for grinding, respectively. Although energy was not used as a variable in this work, there is sufficient evidence in the literature to correlate the size reduction parameters with grinding energy or to correlate energy with grinding time. For example, a study on suspensions using a wet grinding process in stirred media mill found similar behavior between the median size of the particles and the grinding time or the specific energy input (the ratio of the total energy supplied to the grinding chamber to the product mass)

(Ouattara and Frances, 2014). The median size rapidly decreases based on time or specific energy input during the first period and then decreases more slowly. This behavior was observed at rotational speeds of 1500, 2000, and 2500 rpm and at solid mass fractions between 0.05 and 0.3. In another work, a high coefficient of determination between the grinding time and energy consumption was observed with an R^2 between 0.88 and 0.99 (Bolaji et al., 2019). This relationship between particle size and grinding time or specific energy input was observed in several works (Hennart et al., 2010; Stenger et al., 2005). Indeed, equation (2) can be rewritten as $K = \alpha\,(E_G\,/P)^{\beta}$, where P is the power rating of the motor, and E_G is the energy consumption during milling.

2.2 Effect of grinding on flotation kinetics

The objective of this step is to observe the effect of grinding time or energy on the flotation kinetics. Therefore, in this step, kinetic flotation tests are performed under different times of grinding. The grinding times selected here, such as P80, are between the particle sizes that we want to analyze. The tests may be conducted in a traditional way (e.g., using a Denver machine (Rahimi et al., 2012; Yianatos and Henríquez, 2006)) or using other methodologies based on the objective of the study (Jeldres et al., 2017). The airflow rate; agitation rate; concentration of collectors and frothers; solid concentration; and other chemical, physical, and machine variables must be fixed based on the condition that is being analyzed.

2.3 Modeling flotation species fractions

The flotation kinetics are modeled considering fine–slow, medium–fast, and coarse–slow species using the following equation:

$$R = R^{\infty}\left[\varphi_{FS}\left(1 - e^{-k_{FS}t_F}\right) + \varphi_{MF}\left(1 - e^{-k_{MF}t_F}\right) + \varphi_{CS}\left(1 - e^{-k_{CS}t_F}\right)\right] \quad (3)$$

$$\varphi_{FS} + \varphi_{MF} + \varphi_{CS} = 1 \quad (4)$$

where R and R^{∞} are the recoveries at flotation time t_F and infinite, respectively. The recovery is a function of the grinding time and flotation time, $R = f(t_G, t_F)$. The parameters φ_{FS} , $\varphi_{MF}, \varphi_{CS}$ are the mass fraction of fine–slow, medium–fast, and coarse–slow species, respectively, which are a function of the grinding time. The kinetic constants, k_{FS}, k_{MF}, k_{CS} are only functions of the type of mineral. This model can be considered an extension of the Kelsall (1961) model, where the slow fraction has been divided into two fractions that indicate the fine and coarse particle sizes. In addition, R^{∞} has been added because studies on the Kelsall model with and without R^{∞} have shown that better results are obtained by including this parameter (Stanojlović and Sokolović, 2014).

Additional equations related to the mass balance between the initial and final mass fractions of the grinding process must also be added. Figure 2 illustrates the nomenclature used and the idea behind the modeling. Let us assume that the species fractions at the initial point are φ_{FS}^{I} , φ_{MF}^{I}, and

φ_{CS}^{I}. Let us also assume that the fraction of coarse–slow that transforms into medium–fast and fine–slow is $\gamma_{CS,MF}$, and $\gamma_{CS,FS}$, respectively. Moreover, the fraction that transforms from medium–fast to fine–slow ($\gamma_{MF,FS}$) is required. The others fractions, such as coarse–slow to coarse–slow, can be expressed as a function of the other fraction (e.g., $\gamma_{CS,CS} = 1 - \gamma_{CS,MF} - \gamma_{CS,FS}$). Then, the following equations give the final species fractions:

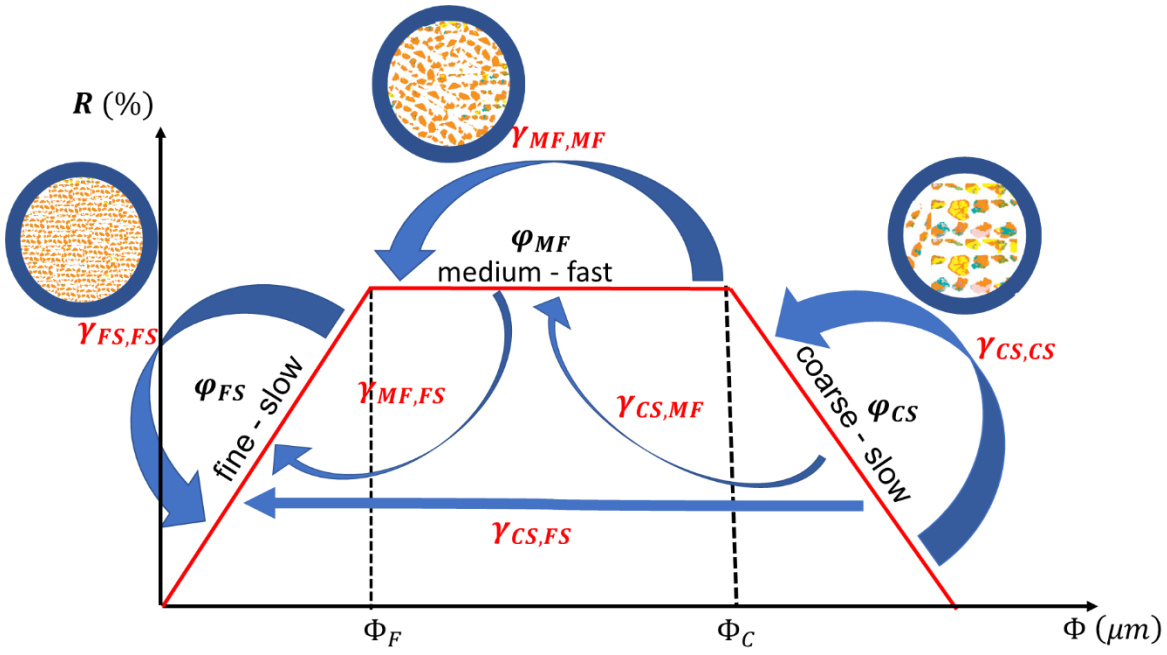

Figure 2. Transformation of the species in the grinding unit.

$$\varphi_{CS}^{F} = \left(1 - \gamma_{CS,MF} - \gamma_{CS,FS}\right) \varphi_{CS}^{I} \tag{5}$$

$$\varphi_{MF}^{F} = \left(1 - \gamma_{MF,FS}\right) \varphi_{MF}^{I} + \gamma_{CS,MF}\, \varphi_{CS}^{I} \tag{6}$$

$$\varphi_{FS}^{F} = \varphi_{FS}^{I} + \gamma_{CS,FS}\, \varphi_{CS}^{I} + \gamma_{MF,FS}\, \varphi_{MF}^{I}. \tag{7}$$

The model parameters are determined by solving the following optimization problem:

$$\min_{k_{FS},k_{MF},k_{CS},R^{\infty},\Phi_S,\Phi_C,\gamma_{CS,MF},\gamma_{CS,FS},\gamma_{MF,FS}} \sum_{t_G} \sum_{t_F} \left(R_{t_G,t_F}^{exp} - R_{t_G,t_F}^{cal}\right)^2 \tag{8}$$

$s.a.$

$$R_{t_G,t_F}^{cal} = R^{\infty}\left[\varphi_{FS,t_G}\left(1 - e^{-k_{FS}t_F}\right) + \varphi_{MF,t_G}\left(1 - e^{-k_{MF}t_F}\right) + \varphi_{CS,t_G}\left(1 - e^{-k_{CS}t_F}\right)\right]$$

$$\varphi_{FS,t_G} + \varphi_{MF,t_G} + \varphi_{CS,t_G} = 1$$

$$P\left(\Phi_{t_G}\right) = 1 - \exp\left(-\left(\frac{\Phi_{t_G}}{K}\right)^{n}\right)$$

$$K = \alpha\, t_G^{\beta}$$

$$\varphi_{FS,t_G} = P\left(\Phi_{t_G}\right)_{\Phi_{t_G}=\Phi_F} \tag{9}$$

$$\varphi_{CS,t_G} = 1 - P\left(\Phi_{t_G}\right)_{\Phi_{t_G}=\Phi_C}$$

$$\varphi_{CS,t_G} = \left(1 - \gamma_{CS,MF} - \gamma_{CS,FS}\right) \varphi_{CS}^{I}$$

$$\varphi_{MF,t_G} = \left(1 - \gamma_{MF,FS}\right) \varphi_{MF}^{I} + \gamma_{CS,MF}\, \varphi_{CS}^{I}$$

$$\varphi_{FS,t_G} = \varphi_{FS}^{I} + \gamma_{CS,FS}\, \varphi_{CS}^{I} + \gamma_{MF,FS}\, \varphi_{MF}^{I}$$

where R_{t_G,t_F}^{exp} and R_{t_G,t_F}^{cal} are the experimental and calculated recoveries, respectively. Moreover, all variables are positive, and the fractions must be between 0 and 1. The parameters $k_{FS}, k_{MF}, k_{CS}, R^{\infty}, \Phi_F, \Phi_C, \varphi_{CS,t_G}, \varphi_{MF,t_G}, \varphi_{FS,t_G}, \varphi_{CS}^{I}, \varphi_{MF}^{I}, \varphi_{FS}^{I}$ are determined with the optimization problem. Note that $\varphi_{CS}^{I}, \varphi_{MF}^{I}, \varphi_{FS}^{I}$ are not known because these fractions depend on the definition of Φ_F, Φ_C, which depends on the flotation kinetics. The particle size Φ_F represents the size under which a particle is considered to behave as fine–slow. In the same way, Φ_C represents the size over which a particle is considered to behave as coarse–slow. These parameters are considered here as adjustable, but it is also possible to determine them based on flotation tests by particle size. This option is not proposed here because the objective is to develop a model with a minimum of experimental tests. The particles between the sizes Φ_c and Φ_F behave as medium–fast species. The problems in Equations 8 and 9 can be solved using commercial software. In summary, the present model includes equations 3 to 7 and a model for the particle size distribution (see equation 1 or 12).

3. Case study

Sulfurized copper ore from the copper mining industry in the Antofagasta region of Chile was used as a case study. The mineral, which features 100% granulometry down to a 10-mesh sieve (2 mm), has an average density of 2.60 g/mL, which was determined by employing a pycnometer and an electronic scale (model LT5001E). The mineralogical composition of the sulfide copper ore is presented in Table 1, where it can be seen that the mineral contains chalcocite and covelite, as well as pyrite as a non-valuable sulfide mineral. The ore has an average copper grade of 0.38% and an average iron grade of 0.76%, as determined by chemical and QEMSCAN analyses.

A 6-hole rotary cutter (the Labtech Herbro model) was used to homogenize and cut the ore samples for the purpose of obtaining representative samples. The ore milling was carried out in a ball mill coupled to a Labtech Hebro model roller using 10 kg steel balls of different sizes for milling (13 balls of 1.5”, 29 balls of 1.25”, 28 balls of 1”, and 45 balls of ¾”). A FAITHFUL brand furnace was

used to dry the samples, which were subjected to a granulometric analysis using an ADVANTECH DuraTapTM Ro-tap for the purpose of determining the feed F80 (the 80% passing size of the feed) and obtaining the mineral particle size distribution data with respect to time. Determination of the distribution of the particle size of the feed and of the samples obtained from the grinding tests was carried out using 8-inch sieve models (ATM PRODUCTS-HEBRO) composed of a series of meshes of different sizes (600, 425, 300, 212, 150, 106, 90, 75, 53, and 45 µm).

Flotation tests were carried out in a METSO flotation cell using a 3300 mL capacity cell. In each flotation test, approximately 1500 g of ore sample was used. In addition, the pH was adjusted to 10.5 using lime, which also serves the purpose of depressing pyrite. An MX7020 collector was used (10 g ton^{-1}) to transform the hydrophilic surfaces of the copper sulfides present in the mineral into a hydrophobic state, and an Math-Froth 202 frother (20 g ton^{-1}) was used to decrease the surface tension between the bubble and the liquid phase of the flotation pulp. At the end of the conditioning period, the stirring speed of the impeller was adjusted to 1000 rpm, and gaseous air was introduced at a flow rate of 6 L min^{-1}. Then, the flotation kinetics were measured, collecting five samples of the concentrate at different times (1, 3, 5, 8, and 12 minutes) and scraping the foam into a container every 10 seconds. Minerals undergoing one minute of grinding will be considered here as minerals without grinding or the initial condition.

Table 1. Mineral composition (QEMSCAN).

Mineral	**% wt/wt**	**Mineral**	**% wt/wt**
Chalcocite/Digenite/Covellite	0.42	Other Fe Oxides/Sulfates	0.26
Chalcopyrite/Bornite	0.08	Quartz	24.44
Enargite/Tennantite/Tetrahedrite	0.00	Feldspars	58.66
Native Cu/Cuprite/Tenorite	0.00	Kaolinite Group	1.88
Other Cu Minerals	0.38	Muscovite/Sericite	0.74
Pyrite	0.68	Chlorite/Biotite	10.87
Molybdenite	0.01	Other Phyllosilicates	0.92
Magnetite	0.11	Others	0.53
Goethite	0.01		
Total			100.00

4. Results

The particle size distribution is shown in Figure 3 after 5, 10, 15, 22, 35, and 40 min of grinding; each grinding time was performed in duplicate. For each grinding time, the particle size distribution was adjusted with Equation 1, using the minimum of the sum of the squared deviations as the objective function. The n value featured no significant changes; it remained constant and equal to 1.0166 throughout. The K values obtained are shown in Figure 4. The K values were adjusted using Equation 2, given $\propto$ = 527.39 and β = -0.684, with an R^2 of 0.9952. In other words, variation in the

K values can be explained in 99.52% of cases for variation in the grinding time using Equation 2. All parameters were fixed using the solve option in Microsoft Excel. After the model was developed, the root-mean-square-deviation of $P(\phi)$, $RMSD = \sqrt{\sum(P^{exp} - P^{cal})^2/N}$, was determined for the distribution function, giving a value of 2.3%, which indicates an adequate representation of the data considering the experimental errors. The experiments were performed in duplicate with a mean deviation of 1.9% and a maximum deviation of 4.2%. The model results are shown in Figure 3, which shows that the highest deviation occurs at 5 minutes of grinding, which is expected for the RRB model.

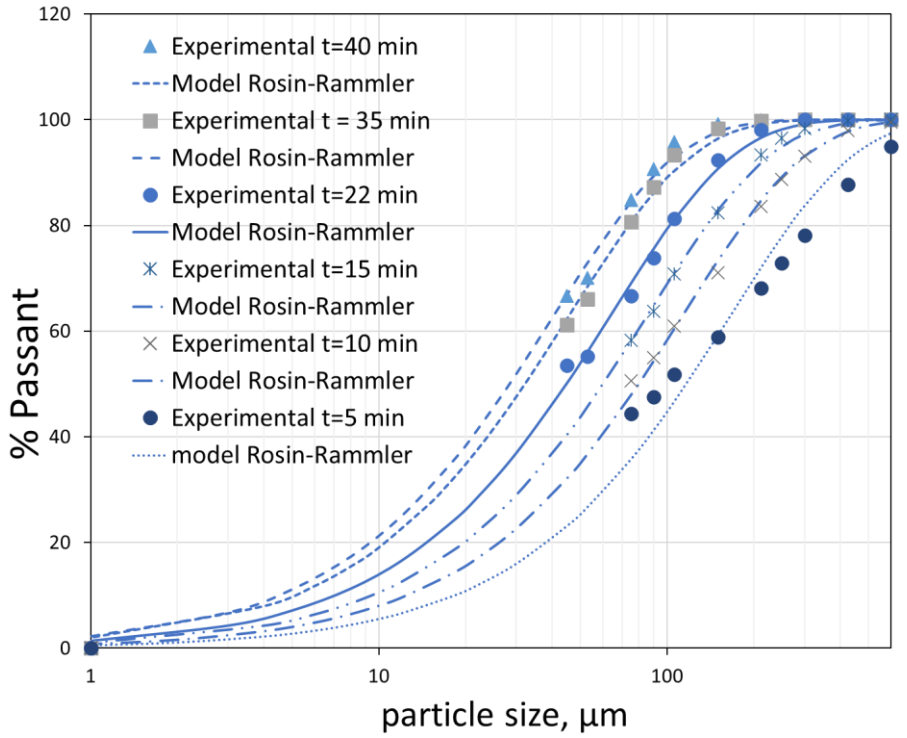

Figure 3. Particle size distribution and the Rosin–Rammler–Bennett (RRB) model.

The results of copper and iron recovery as a function of time are shown in Figure 5 for 1, 2, 4, 8, and 12 minutes of grinding. Both copper and iron were measured at flotation times of 1, 3, 5, 8, and 12 minutes. The copper and iron recoveries increased as the grinding time increased because there was greater liberation of the mineral.

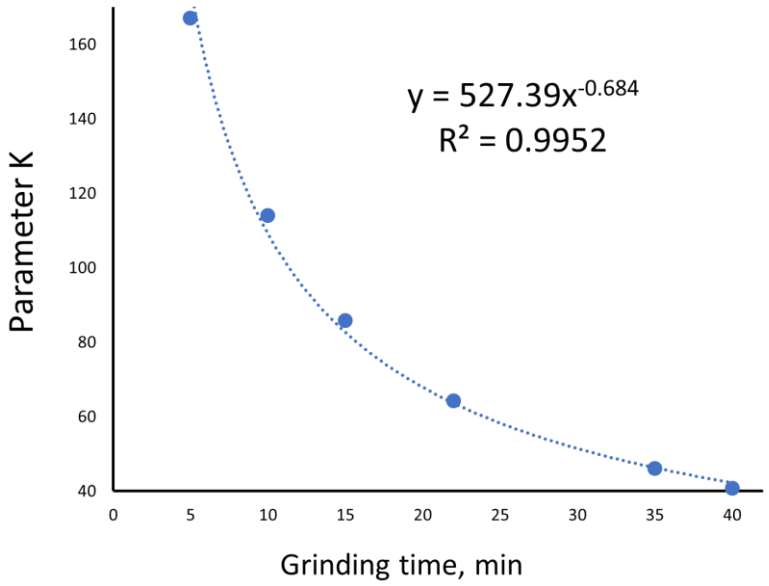

Figure 4. Adjusted K values in Equation 2.

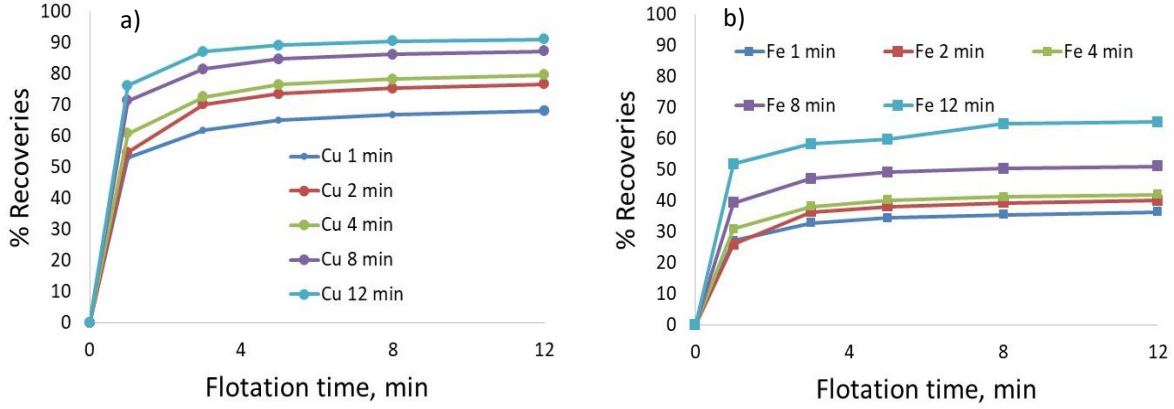

Figure 5. Experimental recoveries of copper (a) and iron (b) at different grinding times.

Using the data shown in Figures 3 and 5, the problems of Equations 8 and 9 were solved using the solve complement in Microsoft Excel for copper recovery as an objective function. Then, the kinetic parameters were determined for iron using the grinding results obtained for copper. Tables 2 and 3 and Figure 6 present the results of this process. Table 2 shows the flotation kinetic parameters together with the RMSD and average absolute deviation (AAD), where $AAD = \sum|R^{exp} - R^{cal}|/N$. Table 3 gives the grinding parameters obtained, which were considered the same for both copper and iron. Figure 6 compares the experimental copper and iron recoveries with the calculated values. Here, the particle sizes that divide the types of species are $\Phi_F = 35\ \mu m$ and $\Phi_C = 374\ \mu m$. The values of RMSD and AAD are greater for iron than for copper. There are several reasons for this difference. First, the grinding parameters were first adjusted for copper, and then the same parameter values were considered for iron. Considering that copper and iron have

different hardness values, different size distributions are to be expected. On the other hand, 28% of the iron comes from oxides that do not provide true flotation but can be recovered by entrainment, which is not considered in this model.

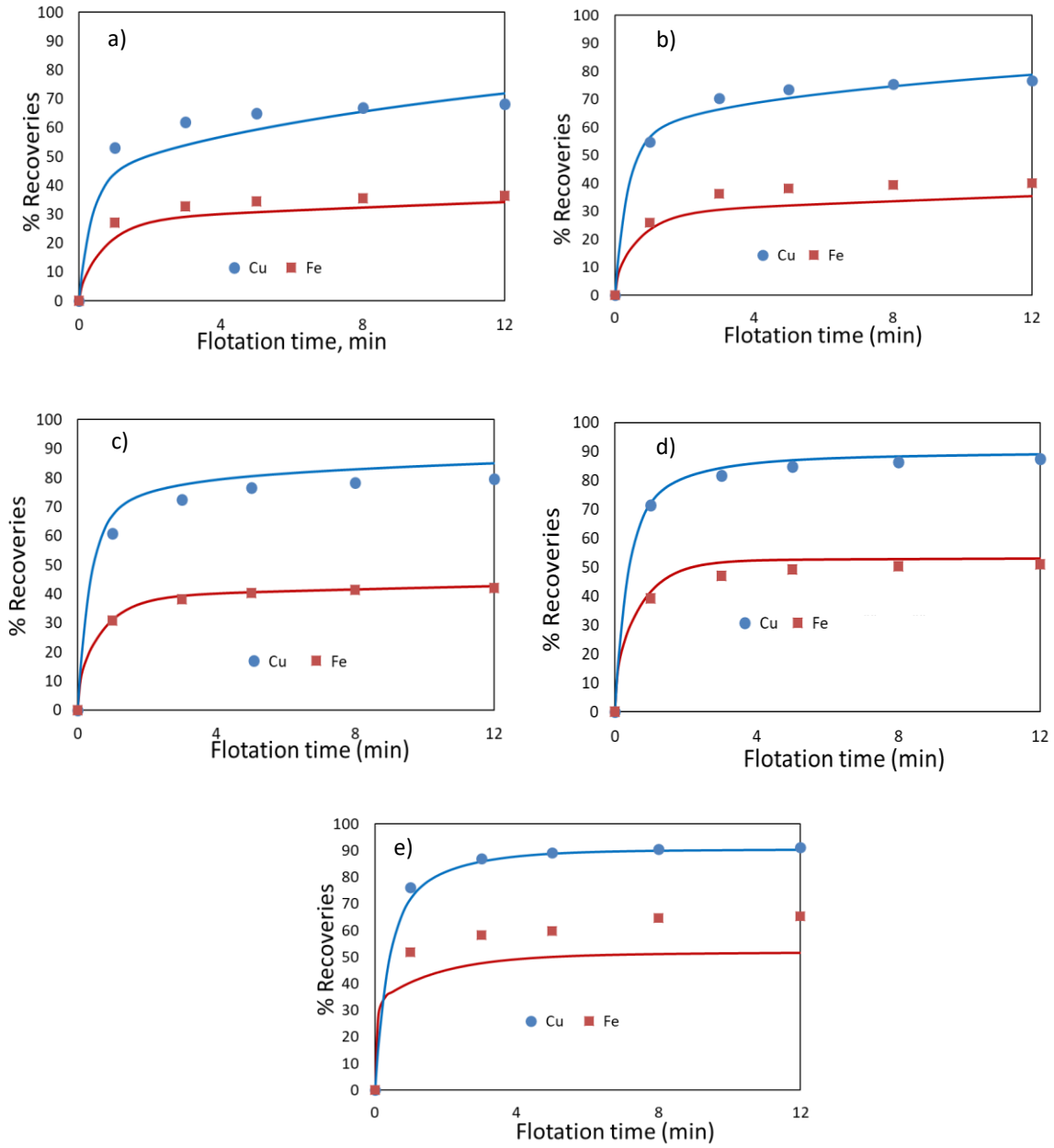

Figure 6. Experimental and calculated recoveries of copper and iron at grinding times of a) 1 min, b) 2 min, c) 4 min, d) 8 min, and e) 12 min.

Table 2. Flotation kinetic parameters.

Parameter	Copper	Iron
R^{∞} [%]	91.00	54.90
k_{FS} [min^{-1}]	0.6590	1.5142
k_{CS} [min^{-1}]	0.0715	0.0227
k_{MF} [min^{-1}]	2.8746	1.6142
$RMSD$ [%]	3.2	4.9
AAD [%]	2.4	3.9

Table 3. Grinding parameters.

Grinding time [min]	Species fractions			Fractional transformation		
	φ_{FS,t_G}	φ_{CS,t_G}	φ_{MF,t_G}	$\gamma_{CS,MF}$	$\gamma_{CS,FS}$	$\gamma_{MF,FS}$
1	0.0615	0.4939	0.4446	-	-	-
2	0.0976	0.3191	0.5833	0.3532	0.0007	0.0805
4	0.1533	0.1573	0.6895	0.5682	0.1134	0.0805
8	0.2361	0.0500	0.7138	0.6265	0.2722	0.0905
12	0.3003	0.0189	0.6808	0.6896	0.2722	0.2348

5. Discussion

The results obtained represent the experimental copper and iron recovery values. In general, the model predicts that the recovery of both copper and iron increases as grinding and flotation times increase (Figure 7). Moreover, the kinetic constant values are in agreement with their definitions—that is, medium–fast species have higher values than the other species, and the coarse–slow species are the slowest. Figure 8 shows the contributions of each of these flotation kinetics for grinding times of 1 and 12 minutes. For a grinding time of 1 minute, the kinetic contribution follows a medium–fast > coarse–slow > fine–slow order because there are more coarse particles than fine particles. Inversely, for a grinding time of 12 minutes, the kinetic contribution follows a medium–fast > fine–slow> coarse–slow order because there are more fine particles than coarse particles. However, at both grinding times, the contribution of medium–fast species is more important. This can also be observed in Table 3, columns 2–4, where the fine–slow species increase with grinding time, whereas the coarse–slow species follow the opposite behavior. The medium–fast species increase with grinding time until reaching a time of 8 minutes and then decrease as this species transforms into a fine–slow species.

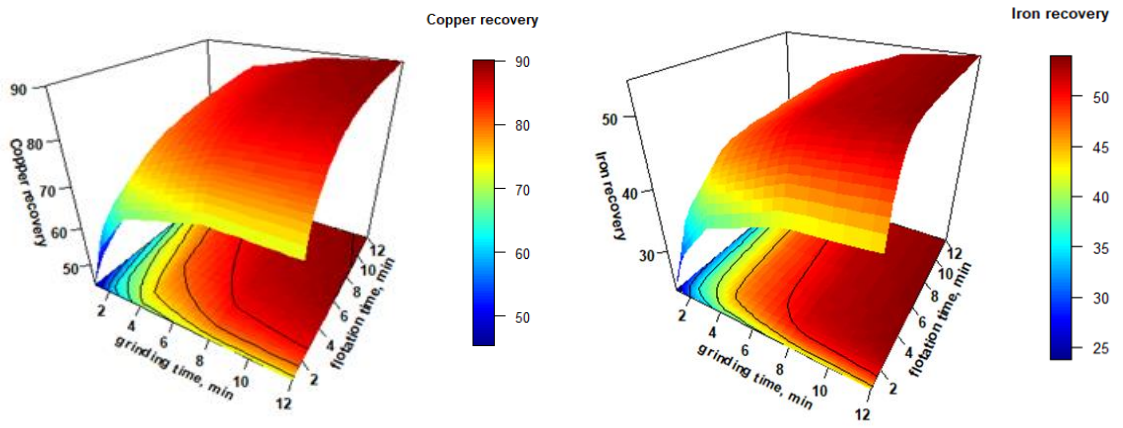

Figure 7. Copper and iron recovery behavior as a function of grinding and flotation time.

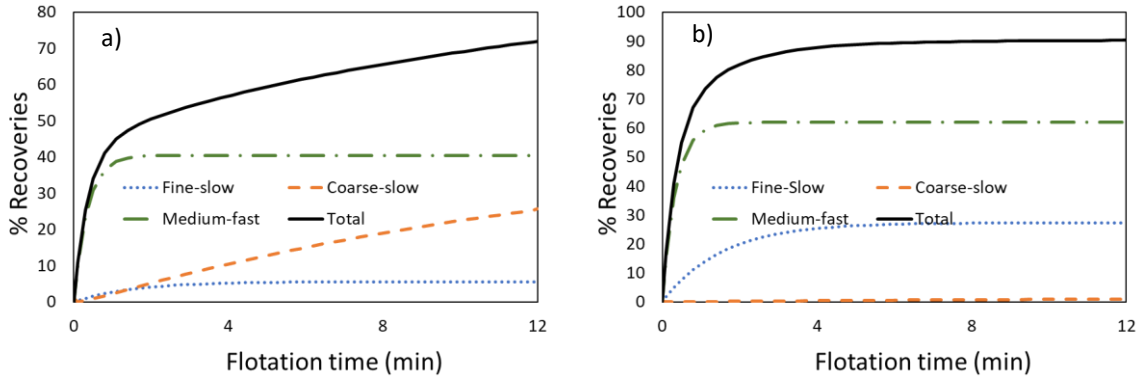

Figure 8. Flotation kinetic contributions for copper recovery at 1 min (a) and 12 min (b) of grinding.

Here, the particle sizes that divide the types of species are $\Phi_F = 35\ \mu m$ (fine–slow species are below that size) and $\Phi_C = 374\ \mu m$ (coarse–slow species have sizes over this size). Values of 35 µm for the fine limits and 374 µm for the coarse fraction limits were determined using the optimization problem. To analyze whether these values are reasonable, the copper and iron recoveries were determined as a function of particle size. Experimental tests were performed under 4 and 12 minutes of grinding, the results of which are shown in Figure 9. The vertically segmented lines in Figure 9 represent values of 35 µm for the fine fraction limits and 374 µm for the coarse fraction limits. Based on the results observed in Figure 9, the particle sizes that divide the types of species, as determined by the optimization program, are consistent. Moreover, Figure 9 clearly indicates that fine–slow particles feature better recoveries than the coarse–slow species for both copper and iron minerals. This behavior agrees with the kinetics constant, where fine–slow species have higher values than coarse–slow species (see Table 2). Figure 10 shows the copper and iron liberation provided by QEMSCAN analysis for the ore. These results show the percentage of each size and liberation level, so the sample in Figure 10 mostly contains particles over 212 µm. This analysis

should be done for each size range. Thus, for copper (figure 10a), for sizes over 212 µm, there is clearly a high percentage of particles with a low level of liberation (< 20%), although most are found with liberation levels between 80 and 95%. For sizes below 150 µm, most of the particles have over 95% liberation. A similar phenomenon was observed for pyrite (Figure 10b): Despite having sizes over 212 µm, fewer pyrite particles featured low liberation. Although the liberation of copper and pyrite does not present the same behavior, these behaviors are not extremely different. Therefore, the assumption regarding the presence of the same fraction of flotation species is acceptable.

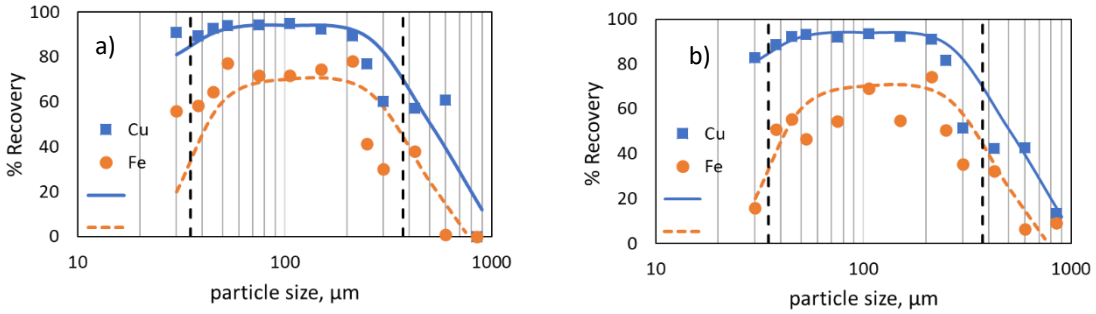

Figure 9. Recoveries versus particle sizes at grinding times of (a) 4 min and (b) 12 min.

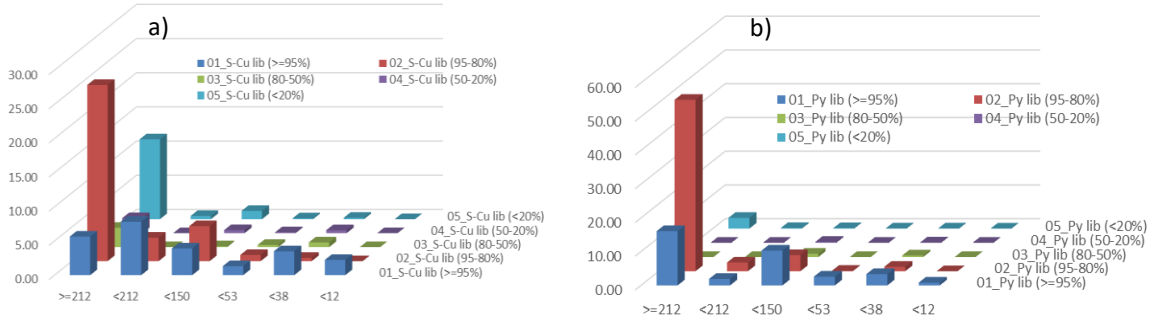

Figure 10. QEMSCAN liberation analysis for (a) copper and (b) pyrite.

After determining the model parameters, the grinding model was developed using equations 1, 2, 5, 6, and 7. The transformation fractions are calculated by solving the equation system given by equations 5, 6, and 7. For simplicity, a metamodel can be developed to avoid these calculations. For example, in the case study, the transformation fraction from coarse–slow to medium–fast, $\gamma_{CS,MF}$, can be correlated with grinding time by using the data from Table 3 with an exponential equation, $\gamma_{CS,MF} = 0.6911\ (1 - e^{-0.3589\, t_G})$, featuring an $RMSD$ of 0.025. Then, the values of the transformation fraction, $\gamma_{CS,FS}$ and $\gamma_{MF,FS}$, are determined using equations 10 and 11. Unlike the values in Table 3, these values have an $RMSD$ of 0.026:

$$\gamma_{CS,FS} = 1 - \gamma_{CS,MF} - \frac{\varphi_{CS,t_G}}{\varphi^I_{CS}} \quad (10)$$

$$\gamma_{MF,FS} = 1 - \frac{\varphi_{MF,t_G}}{\varphi^I_{MF}} + \gamma_{CS,MF}\frac{\varphi^I_{CS}}{\varphi^I_{MF}}. \quad (11)$$

The model has different potential applications, including the design, operation, and analysis of flotation circuits. For example, Table 3 shows that the fraction of medium–fast particles reaches its maximum at 8 minutes of grinding time and then decreases at 12 minutes. This result indicates that the optimum grinding time is between 8 and 12 minutes. On the other hand, Figure 7 shows that several combinations of grinding times and flotation times can produce the same result in copper recovery. These contour plots can thus be used to analyze the best combinations of grinding and flotation time. Notably, numerical methods, such as simulation and optimization, can be used for this purpose based on one or more objective functions. These applications, however, are outside of the scope of this manuscript.

5.1 Uncertainty and sensitivity Analyses.

The development of a model must consider verification, validation, and uncertainty quantification (Chapurlat and Braesch, 2008; Lane and Ryan, 2018; Lucay et al., 2020; Mellado et al., 2018). The goal of verification is to detect any mistakes and prevent any misunderstandings concerning the interpretation of a given model. On the other hand, the goal of validation is to demonstrate that the model is an accurate and relevant representation of reality. These activities were presented in the previous sections. Uncertainty quantification is used for providing a general overview of the effect of uncertainties on the response of a model. Generally, uncertainties are broadly classified into stochastic and epistemic uncertainty. Stochastic uncertainty describes the natural or intrinsic variability of a quantity of interest (e.g., particle size). Epistemic uncertainty represents the lack of knowledge (e.g., whether the values of the model parameters are true). Here, the true values of the model are not known, and only estimated values were calculated. These values depend on experimental data and the numerical optimization method utilized for their calculations. This model is nonlinear, so several local optima exist. Moreover, the numerical method can find a local optimum. Therefore, in this section, uncertainty quantification is performed for the parameters of the present model.

Here, to analyze the variation generated by the uncertainty of the flotation model parameters, uncertainty quantification is performed using uncertainty analysis (UA) and global sensitivity analysis (GSA). UA and GSA are considered appropriate techniques for uncertainty quantification (Lane and Ryan, 2018; Lucay et al., 2020; Mellado et al., 2018; Sullivan, 2015). UA seeks to quantify the uncertainty in output variables as a consequence of uncertainty in the input variables. This analysis is usually carried out in mineral processing and is also used in this study under a Monte Carlo simulation (Mellado et al., 2012; Montenegro et al., 2015). Sensitivity analysis seeks to determine which uncertainties are responsible for the uncertainties in the output variables and is usually done by varying one variable at a time from a specific point. This type of analysis is not

suitable when one intends to analyze the uncertainty in a range of values of input variables. Further, in many complex processes, the input variables interact with each other; therefore, to evaluate the effect of one input variable on the model output, keeping the other input variables constant is inappropriate. Conversely, the GSA is a statistical tool that allows one to quantify the importance of input variables and their interactions on the model output. There are several methods used to perform GSA, but the methods based on variance decomposition give the most appropriate results due to its efficiency and versatility (Gálvez and Capuz-Rizo, 2016). The method of Sobol–Jansen belongs to this category and allows one to calculate the first-order sensitivity index and the total sensitivity index for each input variable of the model (Saltelli et al., 2010). The first order index provides the necessary information to establish the most important input variable. In comparison, the total index provides the necessary information to establish the input variables that do not affect the output variable. Total and first-order indices match when the input variables do not interact with each other. The total Sobol index indicates the relative importance of the uncertainty of an input factor in the system response, where the larger its value is, the more significant its contribution. As determined in (Lucay et al., 2020), the Sobol–Jansen method exhibits good performance when analyzing the processes utilized in mineral processing. Moreover, this method has been applied to mineral processing problems with very good results (Lucay et al., 2015, 2019; Sepúlveda et al., 2014). Consequently, the Sobol–Jansen method is implemented in the present manuscript.

Figure 11 shows the results of the uncertainty analysis for copper and iron recovery at different times of flotation and grinding. To carry out this study, uncertainty was considered using the R^{∞}, k_{FS}, k_{MF} and k_{CS} parameters of the model. The uncertainties of k_{FS}, k_{MF}, and k_{CS} were represented via uniform distributions $\sim U(0.8x, 1.2x)$, where x is the value of the parameters k_{FS}, k_{MF}, and k_{CS}, and the uncertainty of R^{∞} is represented by the uniform distribution $\sim U(0.97x, 1.03x)$. These values were determined via a previous analysis, which allowed us to identify the strong effect of R^{∞} on the recoveries. This observation was corroborated with GSA using the Sobol–Jansen method.

Figure 12 shows the Sobol's indices for different grinding and flotation times. Figure 12a indicates that the uncertainty in the recoveries under an infinite flotation time, R^{∞}, is the most important contribution to uncertainty in copper recovery. Their effect is less significant under low flotation or grinding times. The kinetic constant of the fine–slow fraction is important as the grinding time increases and flotation time decreases (Figure 12b). The kinetic constant of the medium–fast fraction contributes more significantly as grinding time decreases and flotation time increases (Figure 12d). Lastly, the coarse–slow fraction has a small contribution to the uncertainty in copper recovery (Figure 12c). Thus, the kinetic model is strongly influenced by infinite recovery, and the kinetic constant contribution depends on the flotation and grinding times, as expected. The behavior of iron (not shown), moreover, is similar. Figure 13 shows the Sobol's indices for cooper recovery, including uncertainties in the fraction of FS, CS, and MF species at grinding times of one and four minutes. At a grinding time of one minute, the uncertainty in the fraction of coarse–slow

species is clearly the most important parameter. The recovery under an infinite time is the second most significant parameter for a grinding time of one minute and the most important parameter at a grinding time of four minutes. The kinetic constant of the medium–fast species is significant at both one and four grinding times, whereas the fraction of the medium–fast species is significant at one grinding time. Notably, several input variables have a near-zero value, and, therefore, it is not possible to differentiate between these variables in Figure 13. Nevertheless, the most critical information is which variables have the highest values for Sobol's indices.

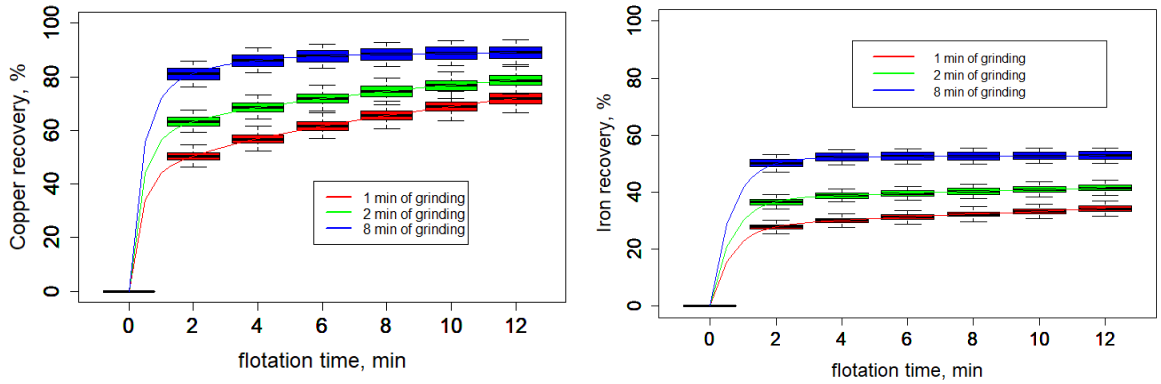

Figure 11. Uncertainties in copper and iron recovery when there are uncertainties of 3% for R^{∞} and 20% for k_{FS}, k_{MF}, and k_{CS} parameters.

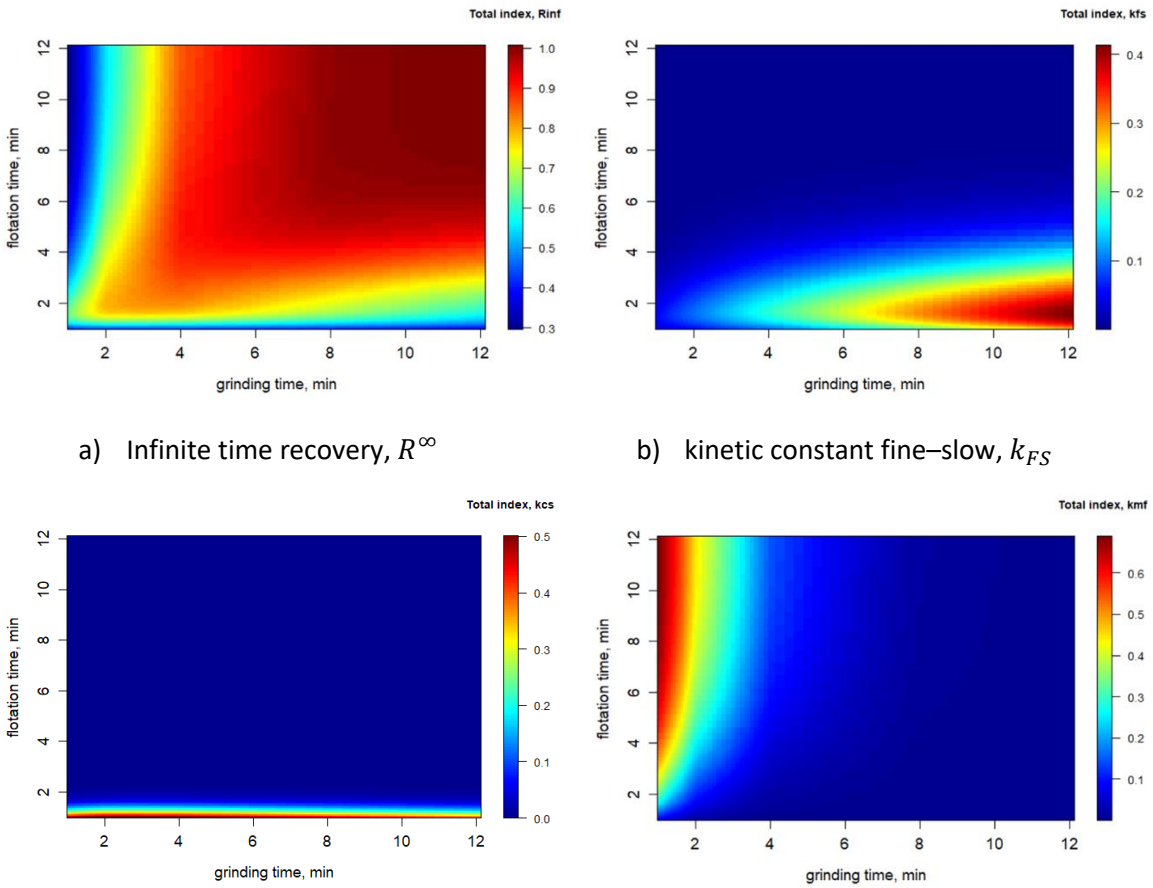

a) Infinite time recovery, R^{∞}

b) kinetic constant fine–slow, k_{FS}

c) kinetic constant coarse–slow, k_{CS}

d) kinetic constant medium–fast, k_{MF},

Figure 12. Sobol's total index for copper recovery (grinding parameter fixed).

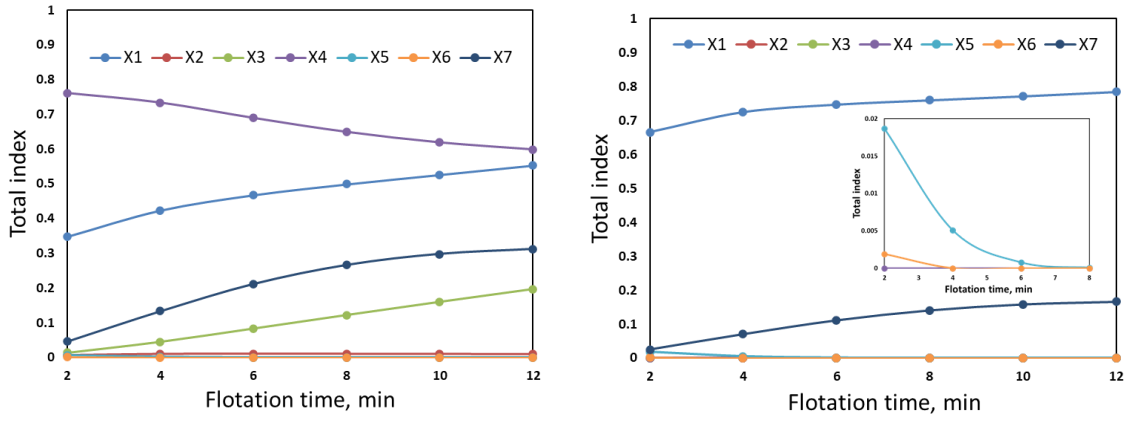

1 min

4 min

Figure 13. Sobol's indices for copper recovery at grinding times of 1 and 4 minutes ($X1 = R^{\infty}$, $X2 = \varphi_{FS,t_G}$, $X3 = \varphi_{MF,t_G}$, $X4 = \varphi_{CS,t_G}$, $X5 = k_{FS}$, $X6 = k_{CS}$, $X7 = k_{MF}$)

5.2 Effect of the particle size distribution model

In this work, the RRB distribution was used to represent the particle size distribution. This size distribution was selected because it is the most well-known and popular distribution function. This distribution function is used in a comprehensive range of applications, including liquid drops, meteorology, emulsification processes, agglomeration, and even astronomical applications (Alderliesten, 2013). This distribution function is also popular in fragmentation processes such as grinding, milling, and crushing operations. For example, in a study on controlling the particle size distribution of the ground carbonate product in stirred media mills, it was found that the profile of the product size distribution from the stirred media mills most closely follows the RRB model (Wang and Forssberg, 2000). In another study, the RRB model was compared with seven mathematical models to describe the particle size distribution in grinding, and it was found that the RRB model best described the size distribution (Shashidhar et al., 2013). However, it is known that the RRB model has some limitations (Alderliesten, 2013). Indeed, the results observed in Figure 3 show some deviations for short milling times.

However, other particle size distribution models can be employed when a more accurate representation is needed or when the RRB model does not perform correctly. There have been many attempts to model particle size distribution. Bayat et al. (2015) studied all developed particle size distribution models using the UNSODA database. This database contains 713 soil samples with a total of 4,174 data pairs. The UNSODA includes a wide range of particles, including clay (0–0.002 mm), silt (0.002–0.05 mm), and sand (0.05–2.0 mm) from different regions around the world. Bayat et al. (2015) found that the Beerkan estimation of the soil transfer model (BEST) (Lassabatère et al., 2006) is flexible and offers high fitting ability over the entire range of particle size distribution. Moreover, the authors determined that BEST was easy to use for soil physics and mechanics research. Thus, in this section, the BEST model is applied as an alternative model to represent particle size distribution as a function of time, and the results are compared with those using the RRB model.

The BEST model can be represented as (Lassabatère et al., 2006):

$$P(\Phi) = \left[1 + \left(\frac{\mathrm{D}_g}{\Phi}\right)^N\right]^{-M} \tag{12}$$

where $P(\Phi)$ is the particle distribution function associated with particle size Φ, M and N are two shape parameters, and D_g is a scale parameter. The results are illustrated in Figure 14, showing clearly better results than the RRB model, with a root-mean-square-deviation of 1.5% (that for RRB was 2.3%). The three BEST parameters were fixed as a grinding time function using the solve option in Microsoft Excel (see Figure 14). These results are not surprising because the BEST model utilizes three parameters that are a function of grinding time (eight constants were adjusted; see Figure 14), whereas RRB uses one constant and one time-dependent parameter (three constants were adjusted). Therefore, a deep analysis is needed to compare both models, which is outside of the aim

of this work. Let us concentrate on the effect of the particle size distribution model on the grinding and flotation modeling. Tables 4 and 5 compare the flotation and grinding modeling using the RRB and BEST models. From the perspective of regression fitting, the RMSD and AAD values for the flotation are close to those for copper, while BEST offers a slightly better fit for iron. The flotation kinetic constant follows the same pattern in both cases: medium–fast > fine–slow > coarse–slow. The particle sizes that divide the type of species were $\Phi_F = 30\ \mu m$ and $\Phi_C = 325\ \mu m$ for BEST model, close to the values obtained when RRB model is applied. Table 5 compares the fraction of medium–fast, fine–slow, coarse–slow species when BEST and RRB are used to represent particle size distribution. The behavior of these fractions follows a similar pattern with grinding time. The major differences are observed over a shorter time, which is logical because the difference between these models is a grinding time below 10 min. In conclusion, the particle size distribution model does not significantly affect the modeling results but introduces uncertainty during its development, which can be quantified via UA and GSA. Figure 13 shows that uncertainties in the grinding parameters have an important contribution under a short grinding time, but flotation kinetic parameter uncertainties are more important under the longest grinding time.

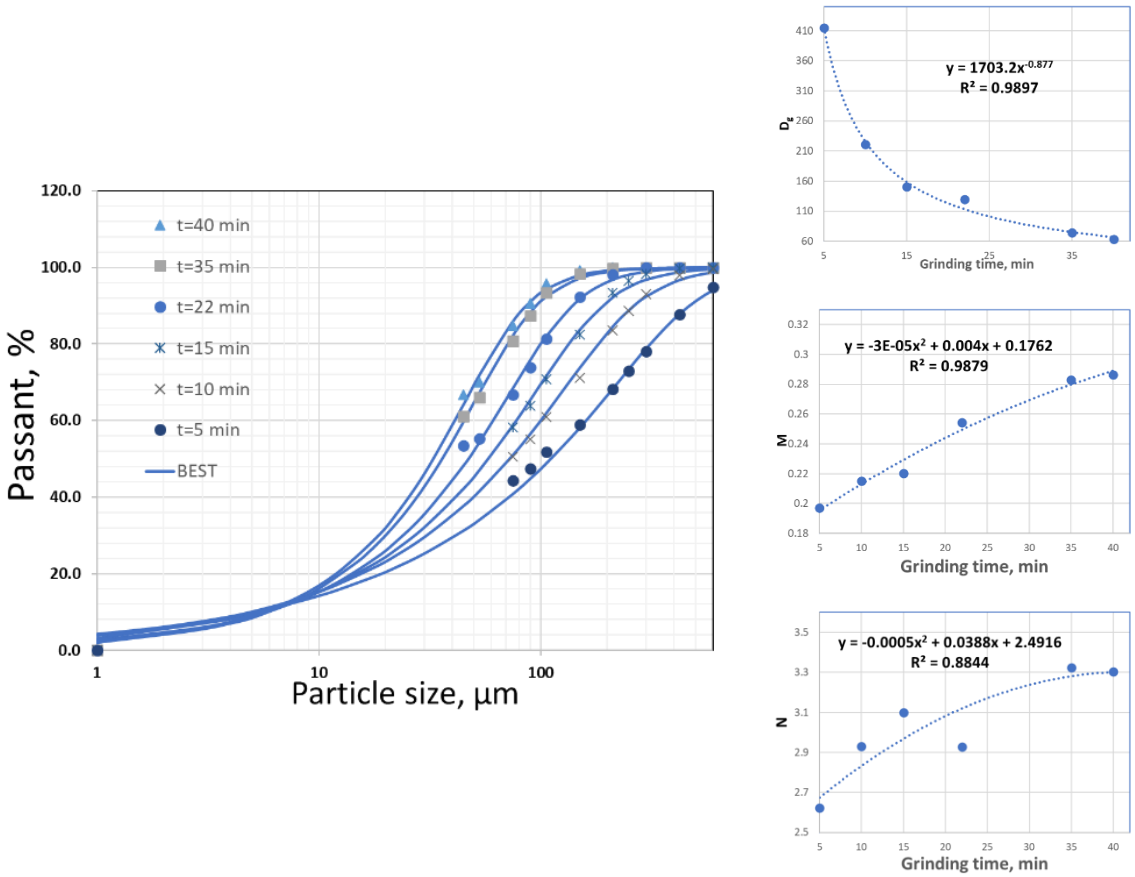

Figure 14. Particle size distribution and Beerkan estimation of the soil transfer model (BEST).

Table 4. Comparison of the flotation kinetic parameters using BEST and RRB for particle size distribution.

Parameter	Copper		Iron	
	RRB	**BEST**	**RRB**	**BEST**
R^{∞} [%]	91.00	92.46	54.90	58.14
k_{FS} [min^{-1}]	0.6590	1.8280	1.5142	0.7689
k_{CS} [min^{-1}]	0.0715	0.0837	0.0227	0.0260
k_{MF} [min^{-1}]	2.8746	2.2280	1.6142	2.7941
$RMSD$ [%]	3.2	3.2	4.9	4.2
AAD [%]	2.4	2.4	3.9	3.3

Table 5. Comparison of the species fractions in grinding when applying BEST and RRB for particle size distribution.

Grinding time [min]	Species fractions, RRB			Species fractions, BEST		
	φ_{FS,t_G}	φ_{CS,t_G}	φ_{MF,t_G}	φ_{FS,t_G}	φ_{CS,t_G}	φ_{MF,t_G}
1	0.0615	0.4939	0.4446	0.1586	0.5315	0.3098
2	0.0976	0.3191	0.5833	0.1976	0.3984	0.4040
4	0.1533	0.1573	0.6895	0.2397	0.2409	0.5195
8	0.2361	0.0500	0.7138	0.2819	0.0960	0.6221
12	0.3003	0.0189	0.6808	0.3070	0.0431	0.6499

6. Conclusions

In this paper, a strategy based on using flotation kinetics to model grinding units was developed with an integrated approach. The methodology allows one to determine the effects of grinding on flotation. The methodology was validated based on its application to a copper sulfide mineral with acceptable results. Given its nature, the application of this model can help preliminary studies on the design, improvement, and simulation of flotation circuits. This model's primary advantage is its simplicity, low cost, and ease of maintenance. The experimental observations of the mineral liberation and flotation behavior of different particle sizes helped to confirm the quality of the model. In addition, uncertainty and sensitivity analyses were applied for uncertainty quantification, thus guaranteeing the robustness of the model developed. Two particle size distribution models were analyzed, RRB and BEST. The BEST model gave the lowest RMSD in the particle size distribution, but similar values of RMSD were observed for flotation modeling. On the other hand, the RRB model used fewer parameters. The main contribution of this work is in providing a new strategy to model grinding for integration into the modeling of flotation circuits. The results obtained suggest that this new strategy of modeling can be extended to other concentration technologies that include grinding.

Acknowledgments

This work was supported by financial assistance from ANID (Fondecyt 1180826). E.M. thanks the Agencia Chilena de Cooperación Internacional para el Desarrollo (AGCID) for the Scholarship for the master's degree. C.C. thanks the Universidad de Antofagasta, grant ANT 1956- MINEDUC. The authors thank Lorena Cortés for her assistance in the experimental tests.

References

Acosta-Flores, R., Lucay, F.A., Cisternas, L.A., Gálvez, E.D., 2018. Two phases optimization methodology for the design of mineral flotation plants including multi-species, bank or cell models. Miner. Met. Process. J.

Acosta-Flores, R., Lucay, F.A., Gálvez, E.D., Cisternas, L.A., 2020. The effect of regrinding on the design of flotation circuits. Miner. Eng. 156, 106524. https://doi.org/10.1016/j.mineng.2020.106524

Agheli, S., Hassanzadeh, A., Hassas, B.V., Hasanzadeh, M., 2018. Effect of pyrite content of feed and configuration of locked particles on rougher flotation of copper in low and high pyritic ore types. Int. J. Min. Sci. Technol. 28, 167–176. https://doi.org/10.1016/j.ijmst.2017.12.002

Alderliesten, M., 2013. Mean Particle Diameters. Part VII. The Rosin-Rammler Size Distribution: Physical and Mathematical Properties and Relationships to Moment-Ratio Defined Mean Particle Diameters. Part. Part. Syst. Charact. 30, 244–257. https://doi.org/10.1002/ppsc.201200021

Asghari, M., Nakhaei, F., VandGhorbany, O., 2019. Copper recovery improvement in an industrial flotation circuit: A case study of Sarcheshmeh copper mine. Energy Sources, Part A Recover. Util. Environ. Eff. 41, 761–778. https://doi.org/10.1080/15567036.2018.1520356

Bayat, H., Rastgo, M., Mansouri Zadeh, M., Vereecken, H., 2015. Particle size distribution models, their characteristics and fitting capability. J. Hydrol. 529, 872–889. https://doi.org/10.1016/j.jhydrol.2015.08.067

Bolaji, O.T., Awonorin, S.O., Sanni, L.O., Shittu, T.A., Adewumi, J.K., 2019. Modeling of particle size distribution and energy consumption of wet milled maize at varying soaking period and method in the production of Ogi. Part. Sci. Technol. 37, 94–102. https://doi.org/10.1080/02726351.2017.1343882

Bu, X., Xie, G., Peng, Y., 2017. Interaction of fine, medium, and coarse particles in coal fines flotation. Energy Sources, Part A Recover. Util. Environ. Eff. 39, 1276–1282. https://doi.org/10.1080/15567036.2017.1323054

Calisaya, D.A., López-Valdivieso, A., de la Cruz, M.H., Gálvez, E.E., Cisternas, L.A., 2016. A strategy for the identification of optimal flotation circuits. Miner. Eng. 96–97, 157–167. https://doi.org/10.1016/j.mineng.2016.06.010

Chapurlat, V., Braesch, C., 2008. Verification, validation, qualification and certification of enterprise models: Statements and opportunities. Comput. Ind. 59, 711–721. https://doi.org/10.1016/j.compind.2007.12.018

Cisternas, L.A., Jamett, N., Gálvez, E.D., 2015. Approximate recovery values for each stage are sufficient to select the concentration circuit structures. Miner. Eng. 83, 175–184. https://doi.org/10.1016/j.mineng.2015.09.003

Cisternas, L.A., Lucay, F.A., Acosta-Flores, R., Gálvez, E.D., 2018. A quasi-review of conceptual flotation design methods based on computational optimization. Miner. Eng. https://doi.org/10.1016/j.mineng.2017.12.002

Delagrammatikas, G., Tsimas, S., 2004. GRINDING PROCESS SIMULATION BASED ON ROSIN-RAMMLER EQUATION. Chem. Eng. Commun. 191, 1362–1378. https://doi.org/10.1080/00986440490472625

Gálvez, E.D., Capuz-Rizo, S.F., 2016. Assessment of global sensitivity analysis methods for project scheduling. Comput. Ind. Eng. 93, 110–120. https://doi.org/10.1016/j.cie.2015.12.010

Gharai, M., Venugopal, R., 2015. Modeling of flotation process – an overview of different approaches. Miner. Process. Extr. Metall. Rev. 37, 08827508.2015.1115991. https://doi.org/10.1080/08827508.2015.1115991

Hennart, S.L.A., Domingues, M.C., Wildeboer, W.J., van Hee, P., Meesters, G.M.H., 2010. Study of the process of stirred ball milling of poorly water soluble organic products using factorial design. Powder Technol. 198, 56–60. https://doi.org/10.1016/j.powtec.2009.10.014

Hennart, S.L.A., Wildeboer, W.J., van Hee, P., Meesters, G.M.H., 2009. Identification of the grinding mechanisms and their origin in a stirred ball mill using population balances. Chem. Eng. Sci. 64, 4123–4130. https://doi.org/10.1016/j.ces.2009.06.031

Hu, W., Hadler, K., Neethling, S.J., Cilliers, J.J., 2013. Determining flotation circuit layout using genetic algorithms with pulp and froth models. Chem. Eng. Sci. https://doi.org/10.1016/j.ces.2013.07.045

Jeldres, R.I., Calisaya, D., Cisternas, L.A., 2017. An improved flotation test method and pyrite depression by an organic reagent during flotation in seawater. J. South. African Inst. Min. Metall. 117. https://doi.org/10.17159/2411-9717/2017/v117n5a12

Jovanović, I., Miljanović, I., 2015. Modelling Of Flotation Processes By Classical Mathematical Methods – A Review. Arch. Min. Sci. 60, 905–919. https://doi.org/10.1515/amsc-2015-0059

Jovanović, I., Miljanović, I., Jovanović, T., 2015. Soft computing-based modeling of flotation processes - A review. Miner. Eng. https://doi.org/10.1016/j.mineng.2015.09.020

Kelsall, D., 1961. Application of probability assessment of flotation systems. Trans. Institut. Min. Met. 70, 191–204.

Kelsall, D.F., 1961. Application of probability in the assessment of flotation systems. Trans. Inst. Min. Metall. 70, 191–20.

King, R.P., 2003. Modeling and Simulation of Mineral Processing Systems, Proceedings of the Institution of Mechanical Engineers, Part E: Journal of Process Mechanical Engineering. Butterworth-Heinemann, Oxford. https://doi.org/10.1177/095440890321700202

Kupka, N., Rudolph, M., 2018. Froth flotation of scheelite – A review. Int. J. Min. Sci. Technol. 28, 373–384. https://doi.org/10.1016/j.ijmst.2017.12.001

Lane, W.A., Ryan, E.M., 2018. Verification, validation, and uncertainty quantification of a sub-grid model for heat transfer in gas-particle flows with immersed horizontal cylinders. Chem. Eng. Sci. 176, 409–420. https://doi.org/10.1016/j.ces.2017.11.018

Lassabatère, L., Angulo-Jaramillo, R., Soria Ugalde, J.M., Cuenca, R., Braud, I., Haverkamp, R., 2006. Beerkan Estimation of Soil Transfer Parameters through Infiltration Experiments-BEST. Soil Sci.

Soc. Am. J. 70, 521–532. https://doi.org/10.2136/sssaj2005.0026

Lucay, F., Cisternas, L.A., Gálvez, E.D., 2015. Global sensitivity analysis for identifying critical process design decisions. Chem. Eng. Res. Des. 103, 74–83. https://doi.org/10.1016/j.cherd.2015.06.015

Lucay, F.A., Gálvez, E.D., Salez-Cruz, M., Cisternas, L.A., 2019. Improving milling operation using uncertainty and global sensitivity analyses. Miner. Eng. 131. https://doi.org/10.1016/j.mineng.2018.11.020

Lucay, F. A., Lopez-Arenas, T., Sales-Cruz, M., Gálvez, E.D., Cisternas, L.A., 2020. Performance profiles for benchmarking of global sensitivity analysis algorithms. Rev. Mex. Ing. Quim. 19, 423–444. https://doi.org/10.24275/rmiq/Sim547

Lucay, Freddy A., Sales-Cruz, M., Gálvez, E.D., Cisternas, L.A., 2020. Modeling of the Complex Behavior through an Improved Response Surface Methodology. Miner. Process. Extr. Metall. Rev. 00, 1–27. https://doi.org/10.1080/08827508.2020.1728265

Mellado, M., Lucay, F., Cisternas, L., Gálvez, E., Sepúlveda, F., 2018. A Posteriori Analysis of Analytical Models for Heap Leaching Using Uncertainty and Global Sensitivity Analyses. Minerals 8, 44. https://doi.org/10.3390/min8020044

Mellado, M.E., Gálvez, E.D., Cisternas, L.A., 2012. Stochastic analysis of heap leaching process via analytical models. Miner. Eng. 33, 93–98. https://doi.org/10.1016/j.mineng.2011.09.006

Meloy, T.P., 1983. Optimizing for grade or profit in mineral processing circuits - Circuit analysis. Int. J. Miner. Process. 11, 89–99. https://doi.org/10.1016/0301-7516(83)90002-9

Mendez, C., de la Fuente, Dagoberto Castillo, J., Reyes, J.L., 2015. Rediseño del circuito de flotación de zinc usando modelación matemática, in: XV Encuentro Sobre Procesamiento de Minerales. San Luis de Potosi, pp. 0–14.

Mendez, D.A., Gálvez, E.D., Cisternas, L.A., 2009. State of the art in the conceptual design of flotation circuits. Int. J. Miner. Process. 90, 1–15. https://doi.org/10.1016/j.minpro.2008.09.009

Monov, V., Sokolov, B., Stoenchev, S., 2012. Grinding in ball mills: Modeling and process control. Cybern. Inf. Technol. 12, 51–68. https://doi.org/10.2478/cait-2012-0012

Montenegro, M.R., Bruckard, W.J., Gálvez, E.D., Cisternas, L.A., 2013. Arsenic-rejection flotation circuit design and selection based on a multiple-objective evaluation. Miner. Eng. 45, 22–31. https://doi.org/10.1016/j.mineng.2013.01.012

Montenegro, M.R., Gálvez, E.D., Cisternas, L.A., 2015. The effects of stage recovery uncertainty in the performance of concentration circuits. Int. J. Miner. Process. 143, 12–17. https://doi.org/10.1016/j.minpro.2015.08.004

Nguyen, A., 2003. Colloidal Science of Flotation, Colloidal Science of Flotation. CRC Press. https://doi.org/10.1201/9781482276411

Noble, A., Luttrell, G.H., Amini, S.H., 2019. Linear Circuit Analysis: a Tool for Addressing Challenges and Identifying Opportunities in Process Circuit Design. Mining, Metall. Explor. 36, 159–171. https://doi.org/10.1007/s42461-018-0031-9

Ouattara, S., Frances, C., 2014. Grinding of calcite suspensions in a stirred media mill: Effect of operational parameters on the product quality and the specific energy. Powder Technol. 255, 89–97. https://doi.org/10.1016/j.powtec.2013.11.025

Pérez-García, E.M., Bouchard, J., Poulin, 2018. Integration of a liberation model in a simulation framework for comminution circuits. Miner. Eng. 126, 167–176. https://doi.org/10.1016/j.mineng.2018.07.009

Polat, M., Chander, S., 2000. First-order flotation kinetics models and methods for estimation of the true distribution of flotation rate constants. Int. J. Miner. Process. 58, 145–166. https://doi.org/10.1016/S0301-7516(99)00069-1

Prakash, R., Majumder, S.K., Singh, A., 2018. Flotation technique: Its mechanisms and design parameters. Chem. Eng. Process. - Process Intensif. 127, 249–270. https://doi.org/10.1016/j.cep.2018.03.029

Rahimi, M., Dehghani, F., Rezai, B., Aslani, M.R., 2012. Influence of the roughness and shape of quartz particles on their flotation kinetics. Int. J. Miner. Metall. Mater. 19, 284–289. https://doi.org/10.1007/s12613-012-0552-z

Saltelli, A., Annoni, P., Azzini, I., Campolongo, F., Ratto, M., Tarantola, S., 2010. Variance based sensitivity analysis of model output. Design and estimator for the total sensitivity index. Comput. Phys. Commun. 181, 259–270. https://doi.org/10.1016/j.cpc.2009.09.018

Sepúlveda, F.D., Cisternas, L.A., Gálvez, E.D., 2014. The use of global sensitivity analysis for improving processes: Applications to mineral processing. Comput. Chem. Eng. 66, 221–232. https://doi.org/10.1016/j.compchemeng.2014.01.008

Sepúlveda, F.D., Lucay, F., González, J.F., Cisternas, L.A., Gálvez, E.D., 2017. A methodology for the conceptual design of flotation circuits by combining group contribution, local/global sensitivity analysis, and reverse simulation. Int. J. Miner. Process. 164. https://doi.org/10.1016/j.minpro.2017.05.008

Shashidhar, M.G., Murthy, T.P.K., Girish, K.G., Manohar, B., 2013. Grinding of Coriander Seeds: Modeling of Particle Size Distribution and Energy Studies. Part. Sci. Technol. 31, 449–457. https://doi.org/10.1080/02726351.2013.772546

Shean, B.J., Cilliers, J.J., 2011. A review of froth flotation control. Int. J. Miner. Process. 100, 57–71. https://doi.org/10.1016/j.minpro.2011.05.002

Sosa-Blanco, C., Hodouin, D., Bazin, C., Lara-Valenzuela, C., Salazar, J., 1999. Integrated simulation of grinding and flotation application to a lead-silver ore. Miner. Eng. 12, 949–967. https://doi.org/10.1016/S0892-6875(99)00080-1

Stanojlović, R.D., Sokolović, J.M., 2014. A Study of the Optimal Model of the Flotation Kinetics of Copper Slag from Copper Mine BOR. Arch. Min. Sci. 59, 821–834. https://doi.org/10.2478/amsc-2014-0057

Stenger, F., Mende, S., Schwedes, J., Peukert, W., 2005. Nanomilling in stirred media mills. Chem. Eng. Sci. 60, 4557–4565. https://doi.org/10.1016/j.ces.2005.02.057

Sullivan, T.J., 2015. Introduction to Uncertainty Quantification, Texts in Applied Mathematics. Springer International Publishing, Cham. https://doi.org/10.1007/978-3-319-23395-6

Sutherland, D.N., 1989. Batch flotation behaviour of composite particles. Miner. Eng. 2, 351–367. https://doi.org/10.1016/0892-6875(89)90004-6

Sutherland, D.N., 1977. An appreciation of galena concentration using a steady-state flotation model. Int. J. Miner. Process. 4, 149–162. https://doi.org/10.1016/0301-7516(77)90022-9

Toneva, P., Peukert, W., 2007. Chapter 20 Modelling of Mills and Milling Circuits. pp. 873–911. https://doi.org/10.1016/S0167-3785(07)12023-6

Varinot, C., Hiltgun, S., Pons, M.-N., Dodds, J., 1997. Identification of the fragmentation mechanisms in wet-phase fine grinding in a stirred bead mill. Chem. Eng. Sci. 52, 3605–3612. https://doi.org/10.1016/S0009-2509(97)89693-5

Wang, Y., Forssberg, E., 2000. Product size distribution in stirred media mills. Miner. Eng. 13, 459–465. https://doi.org/10.1016/S0892-6875(00)00025-X

Williams, M.C., Fuerstenau, D.W., Meloy, T.P., 1986. Circuit analysis—General product equations for multifeed, multistage circuits containing variable selectivity functions. Int. J. Miner. Process. 17, 99–111. https://doi.org/10.1016/0301-7516(86)90048-7

Yianatos, J., Carrasco, C., Bergh, L., Vinnett, L., Torres, C., 2012. Modelling and simulation of rougher flotation circuits. Int. J. Miner. Process. 112–113, 63–70. https://doi.org/10.1016/j.minpro.2012.06.005

Yianatos, J.B., Henríquez, F.D., 2006. Short-cut method for flotation rates modelling of industrial flotation banks. Miner. Eng. 19, 1336–1340. https://doi.org/10.1016/j.mineng.2005.12.010